Electron Transport in Bathocuproine Interlayer in Organic Semiconductor Devices

Hiroyuki Yoshida

Graduate School of Advanced Integration Science, Chiba University
1-33 Yayoi-cho, Inage-ku, Chiba-shi 263-8522, Japan
TEL: +81-43-290-2958
FAX: +81-43-207-3896
E-mail: hyoshida@chiba-u.jp

Abstract

When a thin layer of bathocuproine (BCP) is inserted between the metal electrode and organic layer of organic semiconductor device, the electron injection/collection efficiency at the interface is significantly improved. However, the mechanism of electron transport through the BCP layer has not been clarified yet. In this study, we directly observed the unoccupied electronic states of the Ag/BCP interface using low-energy inverse photoemission spectroscopy. The result shows that Ag strongly interacts with the BCP molecule and the lowest unoccupied molecular orbital (LUMO) level of the Ag-BCP complex aligns with the Fermi level indicating that the electron transport occurs through the LUMO level of the complex. With the aid of DFT calculation, we identify the reaction product.

Introduction

Interface energy level alignment of metal and organic layers is crucial to the performance of organic electronic devices such as organic light emitting diodes (OLEDs), organic field effect transistors, and organic photovoltaic cells (OPVs).[1-5] It has been demonstrated that inserting a thin layer of organic or inorganic material can improve the charge injection/collection efficiencies. Novel insertion layers have been developed and demonstrated to manipulate the relative energy levels at the interface. [6-8]

2,9-Dimethyl-4,7-diphenyl-1,10-phenanthroline (bathocuproine, BCP) is a benchmark of the cathode buffer layer. A thin layer of BCP inserted between a metal cathode and an electron transport layer improves the performances of OLED [9, 10] and OPV [11, 12] significantly. BCP has a large ionization energy of 6.5 eV [13] which is the highest occupied molecular orbital derived-level (HOMO level) with respect to the vacuum level and corresponds to the hole transport level. Thus the BCP layer was initially intended to block the exciton and hole diffusion from the electron transport layer to the cathode.[10]

The insertion of BCP layer also facilitates the electron transport across the cathode and electron transport layer. There are, however, controversial explanations on the mechanism of the electron transport in the BCP layer. The electron transport level, or the lowest unoccupied molecular orbital derived level (LUMO level), of BCP is assumed to locate at 3.0 eV below the vacuum level (i.e. electron affinity) estimated from the ionization energy of 6.5 eV and the optical gap of 3.5 eV as schematically shown in Fig. 1a.[13] Since this is substantially higher than the workfunction of typical cathode materials such as Al and Ag (around 4.5 eV), it was suggested that the electron transport occurs not through the LUMO level of BCP but through the unoccupied levels generated by the metal deposition.[12] In the earlier work, the alignment of the vacuum levels between the BCP layer and metal are conjectured.[9-12]

Ultraviolet photoemission spectroscopy (UPS) studies have revealed a large vacuum level shift at the BCP/metal interface.[14-18] Sakurai and coworkers systematically studied the energy level alignment between the BCP layer and metal surface with different workfunctions such as Au, Cu, Ag, Al, In, Mg and Ca.[14, 15, 17] They observed a constant vacuum level shift of 1.6 eV for the metals with the workfunction higher than 4.3 eV (Au, Cu and Ag), while the vacuum level shift decreases proportional to the workfunciton for those with the workfunciton smaller than 4.3 eV (Ag through Ca). In the latter group of metals, the LUMO level of BCP may align with the Fermi level of the metal as shown in Fig. 1b. Hence, the authors suggested the electron transport through the LUMO level of BCP.

Their UPS results pose several questions. First, the electron affinity of BCP is assumed to about

3.0 eV based on the ionization energy and optical gap. The estimated value using the optical gap is usually 0.2 – 1.0 eV higher than the actual electron affinity due to the exciton binding energy [19-21] meaning that the actual electron LUMO level may be higher than this estimation. Second, the Fermi level of the metal seems to be pinned in the middle of the band gap (at 2.7 eV below the vacuum level) of BCP for the metal with the workfunction smaller than 4.3 eV. Usually the Fermi level of the metal is pinned in the vicinity of either HOMO or LUMO level.[4, 5, 22, 23] The pinning in the middle of the band gap of BCP suggests existence of a gap state though no gap states have been reported in the vicinity of the Fermi level.[14, 15, 17]

The substantial problem of these earlier studies is that energies of the electron transport levels (unoccupied states) are estimated from the experimental data on the occupied states obtained by UPS. In order to discuss the electron transport levels at the organic/metal interface, inverse photoemission spectroscopy (IPES) is in principle the suitable technique because the electron transport level is directly observed and the method is surface sensitive. The previous IPES, however, has serious disadvantages such as radiation damage to organic samples and low energy resolution.

Recently we developed a new method, called low-energy inverse photoemission spectroscopy (LEIPS). [24-26] In this technique, electrons having a kinetic energy below 5 eV are introduced to the sample surface, and photons emitted due to the radiative transition to the unoccupied states are detected. Since the electron kinetic energy is below the damage threshold of organic materials, the sample damage is negligible. By lowering the electron energy, the photon energy falls in the near-ultraviolet range leading to the improvement of the energy resolution by a factor of two. We have demonstrated that the electron affinity of organic materials can be determined with the precision comparable to the ionization energy determined by UPS.[27-32]

Using this technique, we determined the electron affinity of BCP to be 1.9 eV.[30] This value is more than 1 eV smaller than the previously assumed one suggesting that the electron transport through the LUMO level of BCP is unlikely. In this study, we examine the interface electronic structure between BCP and Ag using LEIPS. The results clearly answer the questions about the electron transport across the BCP layer and interface energy level alignment at the BCP/metal.

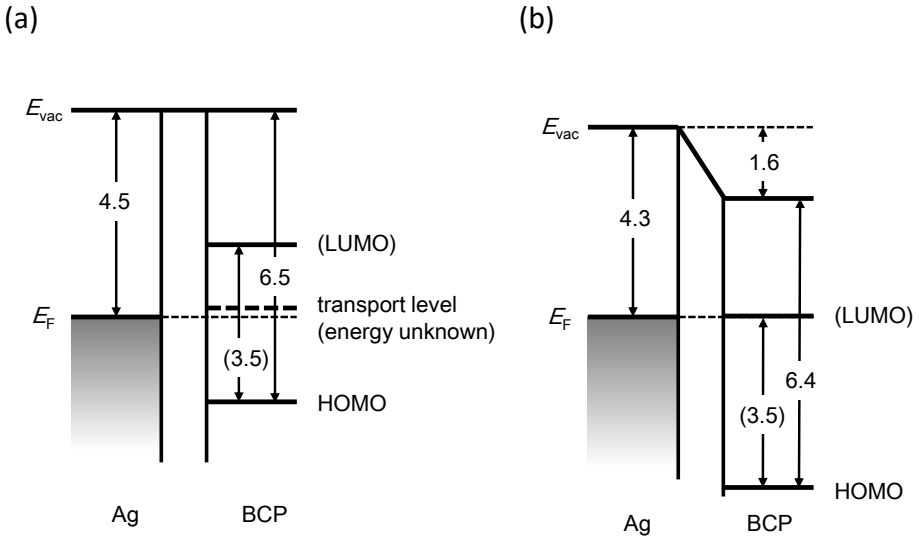

Fig. 1: Energy level diagrams of Ag and BCP interface proposed in Refs. 11 (a) and 17 (b). In these earlier studies, the LUMO levels were estimated from the HOMO level and optical gap.

Experimental

BCP (Aldrich, sublimed grade) was used as received. BCP was vacuum-deposited onto an indium-tin oxide (Flat ITO, Geomatec Co., Ltd.) surface with a thickness of 10 nm at a rate of 1 nm s^{-1}. Then Ag was deposited on the BCP layer and the sample was transferred to the measurement without exposing to air. Detail of the LEIPS apparatus is described elsewhere.[33] The electron beam with the current density of 5-25 x 10^{-2} A m^{-2} was incident to the sample surface and the emitted photons were focused into the photon detector consisting of a bandpass filter (center energy of 4.38 eV or 3.71 eV) and a photomultiplier. Overall energy resolution was about 0.3 eV. No discernible differences were observed depending on the sample current or photon energy confirming that the LEIPS spectra were free from the sample charging. The vacuum level E_{vac} was determined as the peak of first derivative of sample current with respect to the electron energy.

Results

Figure 2 shows the LEIPS spectra and the first derivative of the sample current for the Ag/BCP layers. The spectrum of the pristine BCP is essentially the same as the previous result.[30] The electron affinity was determined based on the standard procedure for the ionization energy determined by UPS. The onset of the LEIPS spectrum is determined as the cross point of the straight line fitted to the onset region of the spectrum and the baseline (see Supplemental Information). The onset is 2.40 eV (Fig. 2a) while the vacuum level E_{vac} is 4.27 eV (Fig. 2b) above

the Fermi level E_F. From the onset energy with respect to E_{vac}, the electron affinity of BCP is determined to 1.87 eV.

When Ag with the average thickness of 0.4 nm is deposited on top of the BCP layer, the spectral line shape completely changes. The tail of the spectrum extends to the Fermi level E_F and the onset of the spectrum shifts by 2.1 eV associated with the decrease of the vacuum level by 1.2 eV. The onset energy of 0.29 eV and the vacuum level of 3.04 eV with respect to E_F gives the electron affinity of 2.75 eV. Such large changes of the spectral line shape as well as of the energy levels suggest strong interaction between the BCP molecule and the Ag atom.

When the average thickness of Ag is further increased to 2.0 and 8.5 nm, the peak energies remain unchanged and the baseline rises. These spectral line shapes can be interpreted as the superposition of the 0.4-nm-thick Ag/BCP and the spectra of pristine metal Ag (displayed by dotted line in Figure 2). The latter component is attributable to the formation of metallic Ag layer or clusters at or near the surface of the BCP layer.

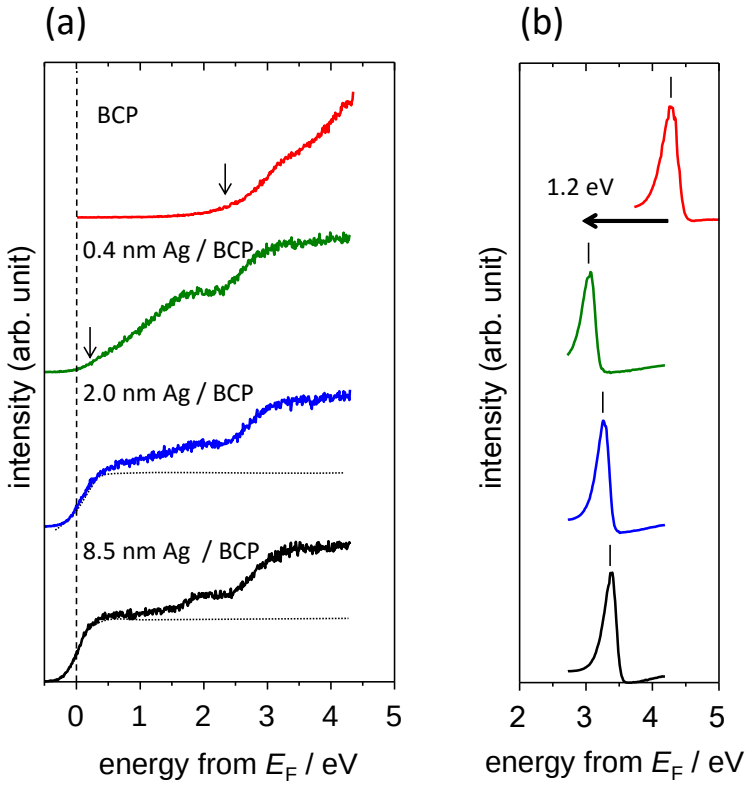

Fig. 2: Experimental results for increasing average thickness of Ag on BCP. (a) LEIPS spectra and (b) first derivatives of sample current show the unoccupied states and the vacuum levels, respectively. The energies are with reference to the Fermi level which is shown by the dashed line. The vertical arrows in panel (a) indicate the onsets of the spectra while the vertical bars show the vacuum levels in panel (b).

In order to elucidate the nature of the strong interaction between BCP and Ag and to identify the reaction product, we carried out the first principle calculation on plausible complexes of BCP and Ag, and compared the results with the experimental spectrum. The calculations were done for an isolated molecule using the hybrid density functional of B3LYP on the Gaussian 09 program.[34] For the basis sets, 6-31G(d) for H, C and O, and Stuttgart/Dresden ECP for Ag are used. The geometry was optimized at the same level.

First, we applied this method to a pristine BCP molecule to assess the reliability of the calculation. The calculated Kohn-Sham orbital eigenvalues were broadened by the Gaussian function with the full width at half maximum (FWHM) of 0.69 eV to simulate the density of states (DOS) which are shown in the upper panel of Figure 3a. The calculated density of states for both the occupied and unoccupied levels are in excellent agreement with the UPS[16] and LEIPS spectra as shown in Figure 3a. Note that the bandgap (the HOMO-LUMO gap) calculated by the B3LYP functional does not reproduce the experimental value correctly. Thus the occupied and unoccupied levels are offseted by about 2 eV in Figure 3.

Now that the UPS/LEIPS spectra of BCP are reproduced by the calculated DOS, the same calculations were made for possible reaction products between a BCP molecule and Ag atom. We tested several candidates as the reaction products. When the Ag atom binds to the nitrogen atoms of BCP as shown in Figure 3b, a stable complex is formed. The binding energy between the BCP and Ag is 0.15 eV calculated as the difference in the total energy. The predicted molecular structure is consistent with the recent X-ray photoemission study on BCP and Mg complex where a strong bond between the nitrogen atoms of BCP and the metal atom was suggested.[35]

The calculated results are compared with the experimental spectra in Figure 3b. For the experimental spectra of BCP and Ag complex, the UPS spectrum of the Ag and BCP co-deposited film with the molar ration of 1.2:1.0 [17] are referred while the LEIPS spectrum of 0.4-nm thick Ag/BCP is shown. The simulated DOSs closely reproduce the experimental ones strongly indicating that a BCP-Ag complex shown in Figure 3b is a dominant reaction product. The occupied DOSs are similar between BCP and BCP-Ag explaining that the previous photoemission studies could not identify the reaction product between BCP and Ag. In contrast, the unoccupied DOS and LEIPS spectrum of BCP is largely affected by the reaction with Ag, which facilitates to identify the reaction product.

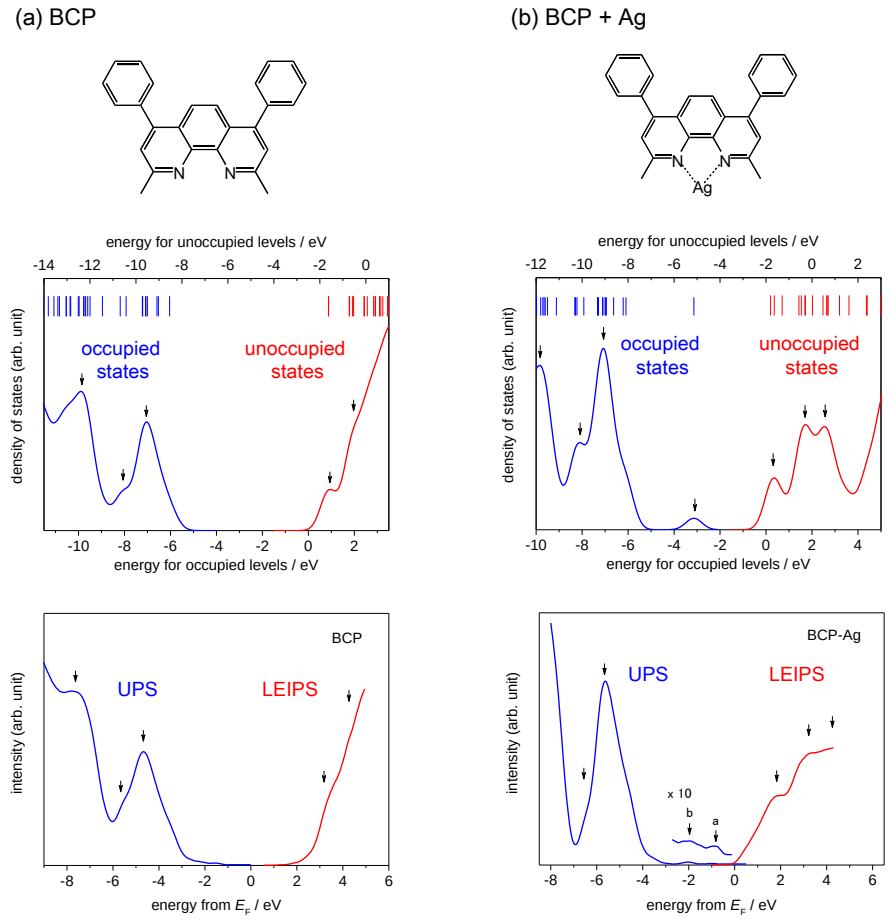

Fig. 3: Molecular structure, calculated Kohn-Sham eigenvalues (vertical bars) and simulated density of states (solid lines) in the upper panels, and the experimental UPS/LEIPS spectra in the lower panels, for a) BCP and b) BCP-Ag complex for the indicated molecular structure. Remarkable spectral features are indicated by the arrows. The UPS spectra of BCP and BCP+Ag are taken from Refs. 16 and 17, respectively.

Figure 4 shows the molecular orbitals of the BCP and BCP-Ag complex. The LUMO and LUMO+1 levels of the complex are almost degenerated, and have little population on the Ag atom. The LUMO and LUMO+1 of BCP-Ag is mainly contributed from the LUMO+1 and LUMO of BCP, respectively. Similarly, the HOMO-1 of BCP-Ag consists mainly of the HOMO of BCP. In contrast, the HOMO of BCP+Ag is localized on Ag atom. The eigenvalue of the HOMO level is -3.14 eV.

In UPS of BCP-Ag, the two gap states peaked at -0.8 eV (peak a in Figure 3b) and -2.0 eV (peak b) with reference to the Fermi level are reported.[14, 17] We tentatively assign the peak b as the HOMO level of BCP-Ag. The HOMO of BCP-Ag is localized on the Ag atom while the HOMO-1 is delocalized over the phenanthroline moiety. In the solid state, the localized orbital is the more effectively screened by the electronic polarization effect resulting in the decrease of the HOMO and

HOMO-1 gap from the calculated gap of 2.95 eV. Usually, the cross section of photoemission is smaller for metal atoms than for organic molecules, which explains the small intensity of the peak b. The peak a may be caused by the partially occupied LUMO level of BCP-Ag. Recent electron spin resonance (ESR) study revealed that electrons are transferred from Al atoms to BCP molecules and anion radicals are formed at the Al/BCP interface.[36] The spin concentration on BCP is estimated to be 1.7%. Assuming the similar magnitude of charge transfer at Ag/BCP interface explains the peak intensity of peak a reasonably. When the concentration of Ag is increased in Ag+BCP co-deposited film, the intensity of the peak a increases [17] which is consistent with our assignment. The LUMO level of BCP-Ag splits to the occupied and unoccupied levels with the difference of about 1 eV. Such increase of the energy gap upon the metal doping is reported in pentacene.[37]

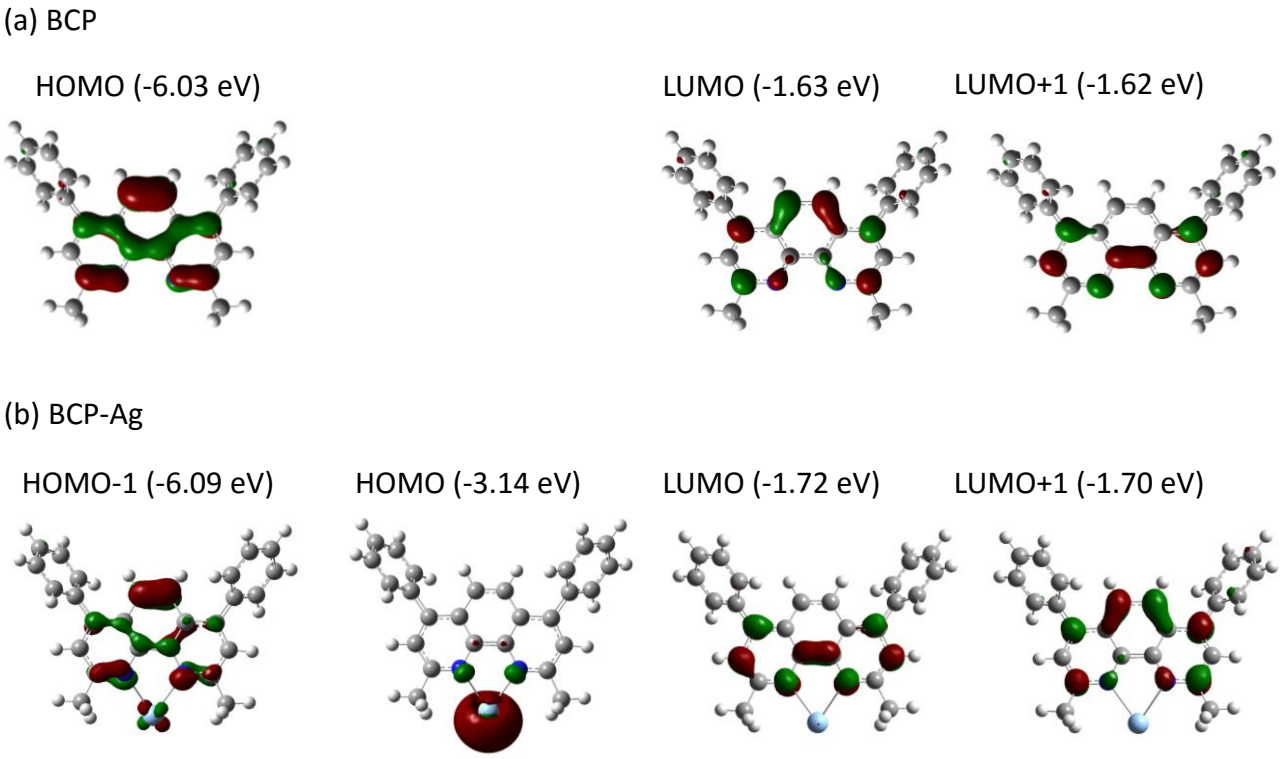

Figure 4: Calculated molecular orbitals and Kohn-Sham eigenvalues for (a) the BCP molecule and (b) the BCP-Ag complex.

Discussion

The results of the present study are summarized in the energy level diagram shown in Figure 5. The workfunction of 4.3 eV is assumed for the Ag overlayer. The vacuum level shift is obtained as the difference in the workfunction between the metal and organic layers. The energy levels are

determined as the onsets of spectra rather than the maxima of peaks because the spectral onset corresponds to the bulk material while the peak to the outermost layer. [38] For example, the HOMO of the BCP and Ag complex is determined to 0.5 eV from the onset of peak a in Figure 3b.

The organic layer may consist of the BCP molecules and BCP-Ag complexes. From the present results, the energy levels of the intact BCP in the mixed organic layer cannot be determined. When the vacuum levels of BCP and Ag align, the difference between the LUMO of BCP and the E_F of Ag exceeds 2 eV. When the vacuum levels of BCP and BCP-Ag aligns, the LUMO level of BCP is 1 eV above the Fermi level and is still too high for the electron transport (Fig. 5). In any cases, it is unlikely that the electron transport occurs through the intact BCP. In contrast, the LUMO level (or more likely the two almost degenerated unoccupied levels, LUMO and LUMO+1) of the BCP-Ag complex is close to the Fermi level through which the electron transport occurs.

The dependence of the thickness of BCP layer on the device performance supports this conclusion. The optimum thickness of BCP layer is reported to be in the range between 5 and 20 nm.[12, 39] When the metal is deposited onto the organic layer, the metal atoms diffuse into the organic layer[3] with the diffusion length ranging from a few to 100 nm.[40-42] It is understandable that the Ag atom diffuses into the BCP layer as much as 20 nm and forms the BCP-Ag complex. When the metal layer is prepared prior to the deposition of BCP layer in the OPV with inverted structure, on the other hand, the pristine BCP layer shows insufficient performance and requires co-deposition with Ag.[43] This further evidences that the electron conduction occurs through the LUMO of the BCP-Ag complex.

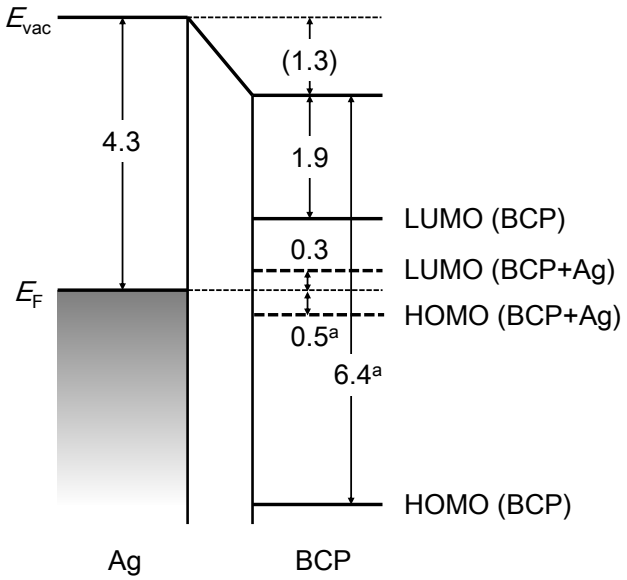

Fig. 5: Energy level diagram of Ag/BCP interface. [a]The values are taken from the photoemission data. [17]

The LUMO level of the BCP-Ag complex is about 0.3 eV above the Fermi level. It is commonly observed that the E_F is pinned about 0.3 eV from the edge of HOMO or LUMO level.[4, 5, 22, 23] The pinning to the LUMO level of BCP-Ag explains the previous UPS results that the Fermi level is pinned in the middle of the bandgap of BCP for metals having the workfuncition lower than 4.3 eV (Ag through Ca).[17] Though the gap state to which the E_F is pinned was not clarified in the previous study, the pinning state is identified as the LUMO level of the BCP-Ag complex in this study. The pinning of E_F to the LUMO level should be associated with the electron transfer from metal to organic layer, which is supported by the ESR study.[36] The BCP and Al (workfunction is about 4.3 eV, showing the pinning) contact gives ESR signal from the anion of BCP while the BCP and Au (workfunction is about 5.1 eV, shows no pinning) contact shows no ESR signal. The authors assumed the formation of BCP anion, but the anion of BCP-metal complex should also give similar ESR signal because the LUMO of BCP-metal complex has a strong character of the molecular orbital of BCP as shown in Figure 4. It is therefore likely that the E_F of Ag is pinned to the LUMO level of BCP-Ag complex.

Conclusion

In this work, we examined the electron transport level at the interface between Ag and BCP using low-energy inverse photoemission spectroscopy (LEIPS). The spectral change upon the Ag deposition on BCP layer suggests the strong interaction between the BCP molecule and Ag atom. The reaction product BCP-Ag is identified with the aid of DFT calculation and the bond energy between BCP and Ag is calculated to be 0.15 eV. The LUMO level of the BCP-Ag complex lies 2.8 eV below the vacuum level and appears to pinned to the Fermi level. On the other hand, the LUMO of pristine BCP is 1 eV above the Fermi level. From these observations, we conclude that the electron transport occurs through the LUMO level of the BCP-Ag complex rather than the intact BCP molecule.

Acknowledgement

This work is supported by KAKENHI Grant Number 26288007 of Japan Society for the Promotion of Science (JSPS) and the Advanced Low Carbon Technology Research and Development Program (ALCA) of the Japan Science and Technology Agency (JST) in part.

References

1. Ishii, H.; Sugiyama, K.; Ito, E.; Seki, K., Energy Level Alignment and Interfacial Electronic Structures at Organic Metal and Organic Organic Interfaces. *Adv. Mater.* **1999,** *11*, 605-625.

2. Koch, N., Organic Electronic Devices and Their Functional Interfaces. *ChemPhysChem* **2007,** *8*, 1438-1455.

3. Hwang, J.; Wan, A.; Kahn, A., Energetics of Metal-Organic Interfaces: New Experiments and Assessment of the Field. *Mater. Sci. Eng. R-Rep.* **2009,** *64*, 1-31.

4. Braun, S.; Salaneck, W. R.; Fahlman, M., Energy-Level Alignment at Organic/Metal and Organic/Organic Interfaces. *Adv. Mater.* **2009,** *21*, 1450-1472.

5. Oehzelt, M.; Koch, N.; Heimel, G., Organic Semiconductor Density of States Controls the Energy Level Alignment at Electrode Interfaces. *Nature Comm.* **2014,** *5*, 4174.

6. Ratcliff, E. L.; Zacher, B.; Armstrong, N. R., Selective Inter Layers and Contacts in Organic Photovoltaic Cells. *J. Phys. Chem. Lett.* **2011,** *2*, 1337-1350.

7. Schlesinger, R.; Xu, Y.; Hofmann, O. T.; Winkler, S.; Frisch, J.; Niederhausen, J.; Vollmer, A.; Blumstengel, S.; Henneberger, F.; Rinke, P., et al., Controlling the Work Function of ZnO and the Energy-Level Alignment at the Interface to Organic Semiconductors with a Molecular Electron Acceptor. *Physical Review B* **2013,** *87*, 155311.

8. Zhou, N.; Kim, M.-G.; Loser, S.; Smith, J.; Yoshida, H.; Guo, X.; Song, C.; Jine, H.; Chen, Z.; Yoon, S. M., et al., Amorphous Oxide Alloys as Interfacial Layers with Broadly Tunable Electronic Structures for Organic Photovoltaic Cells. *Proceedings of the National Academy of Sciences of the United States of America* **2015,** *112*, 7897-7902.

9. Kijima, Y.; Asai, N.; Tamura, S., A Blue Organic Light Emitting Diode. *Jpn. J. Appl. Phys. Part 1 - Regul. Pap. Short Notes Rev. Pap.* **1999,** *38*, 5274-5277.

10. O'Brien, D. F.; Baldo, M. A.; Thompson, M. E.; Forrest, S. R., Improved Energy Transfer in Electrophosphorescent Devices. *Appl. Phys. Lett.* **1999,** *74*, 442-444.

11. Peumans, P.; Bulovic, V.; Forrest, S. R., Efficient Photon Harvesting at High Optical Intensities in Ultrathin Organic Double-Heterostructure Photovoltaic Diodes. *Appl. Phys. Lett.* **2000,** *76*, 2650-2652.

12. Peumans, P.; Forrest, S. R., Very-High-Efficiency Double-Heterostructure Copper Phthalocyanine/C_{60} Photovoltaic Cells. *Appl. Phys. Lett.* **2001,** *79*, 126-128.

13. Hill, I. G.; Kahn, A., Organic Semiconductor Heterointerfaces Containing Bathocuproine. *J. Appl. Phys.* **1999,** *86*, 4515-4519.

14. Toyoshima, S.; Kuwabara, K.; Sakurai, T.; Taima, T.; Saito, K.; Kato, H.; Akimoto, K., Electronic Structure of Bathocuproine on Metal Studied by Ultraviolet Photoemission Spectroscopy. *Jpn. J. Appl. Phys. Part 1 - Regul. Pap. Brief Commun. Rev. Pap.* **2007,** *46*, 2692-2695.

15. Toyoshima, S.; Sakurai, T.; Taima, T.; Saito, K.; Kat, H.; Akimoto, K., Ultraviolet Photoemission Study of Interaction between Bathocuproine and Calcium. *Jpn. J. Appl. Phys.* **2008,** *47*, 1397-1399.

16. Aoki, M.; Toyoshima, S.; Kamada, T.; Sogo, M.; Masuda, S.; Sakurai, T.; Akimoto, K., Level

Alignment of Gap State at Organic-Metal Interface. *J. Appl. Phys.* **2009,** *106*, 043715.

17. Sakurai, T.; Toyoshima, S.; Kitazume, H.; Masuda, S.; Kato, H.; Akimoto, K., Influence of Gap States on Electrical Properties at Interface between Bathocuproine and Various Types of Metals. *J. Appl. Phys.* **2010,** *107*, 043707.

18. Nakayama, Y.; Nguyen, T. L.; Ozawa, Y.; Machida, S.; Sato, T.; Tokairin, H.; Noguchi, Y.; Ishii, H., Complete Demonstration of the Valence Electronic Structure inside a Practical Organic Solar Cell Probed by Low Energy Photoemission. *Adv. Energy Mater.* **2014,** *4*, 1301354.

19. Hill, I. G.; Kahn, A.; Soos, Z. G.; Pascal, R. A., Charge-Separation Energy in Films of π-Conjugated Organic Molecules. *Chem. Phys. Lett.* **2000,** *327*, 181-188.

20. Knupfer, M., Exciton Binding Energies in Organic Semiconductors. *Appl. Phys. A* **2003,** *77*, 623-626.

21. Djurovich, P. I.; Mayo, E. I.; Forrest, S. R.; Thompson, M. E., Measurement of the Lowest Unoccupied Molecular Orbital Energies of Molecular Organic Semiconductors. *Org. Electron.* **2009,** *10*, 515-520.

22. Lange, I.; Blakesley, J. C.; Frisch, J.; Vollmer, A.; Koch, N.; Neher, D., Band Bending in Conjugated Polymer Layers. *Phys. Rev. Lett.* **2011,** *106*, 216402.

23. Yogev, S.; Matsubara, R.; Nakamura, M.; Zschieschang, U.; Klauk, H.; Rosenwaks, Y., Fermi Level Pinning by Gap States in Organic Semiconductors. *Phys. Rev. Lett.* **2013,** *110*, 036803.

24. Yoshida, H., Near-Ultraviolet Inverse Photoemission Spectroscopy Using Ultra-Low Energy Electrons. *Chem. Phys. Lett.* **2012,** *539-540*, 180-185.

25. Yoshida, H., Measuring the Electron Affinity of Organic Solids: An Indispensable New Tool for Organic Electronics. *Analytical and Bioanalytical Chemistry* **2014,** *406*, 2231-2237.

26. Yoshida, H., Principle and Application of Low Energy Inverse Photoemission Spectroscopy: A New Method for Measuring Unoccupied States of Organic Semiconductors. *J. Electron Spectrosc. Relat. Phenom.* **2015,** *204A,* 116-124.

27. Fabiano, S.; Yoshida, H.; Chen, Z. H.; Facchetti, A.; Loi, M. A., Orientation-Dependent Electronic Structures and Charge Transport Mechanisms in Ultrathin Polymeric N-Channel Field-Effect Transistors. *ACS Appl. Mater. Interfaces* **2013,** *5*, 4417-4422.

28. Han, W.; Yoshida, H.; Ueno, N.; Kera, S., Electron Affinity of Pentacene Thin Film Studied by Radiation-Damage Free Inverse Photoemission Spectroscopy. *Appl. Phys. Lett.* **2013,** *103*, 123303.

29. Yoshida, H., Low-Energy Inverse Photoemission Study on the Electron Affinities of Fullerene Derivatives for Organic Photovoltaic Cells. *J. Phys. Chem. C* **2014,** *118*, 24377-24382.

30. Yoshida, H.; Yoshizaki, K., Electron Affinities of Organic Materials Used for Organic Light-Emitting Diodes: A Low-Energy Inverse Photoemission Study. *Org. Electron.* **2015,** *20*, 24-30.

31. Zhong, Y. F.; Izawa, S.; Hashimoto, K.; Tajima, K.; Koganezawa, T.; Yoshida, H., Crystallization-Induced Energy Level Change of 6,6 -Phenyl C_{61}-Butyric Acid Methyl Ester (PCBM) Film: Impact of Electronic Polarization Energy. *J. Phys. Chem. C* **2015,** *119*, 23-28.

32. Yoshida, H.; Yamada, K.; Tsutsumi, J.; Sato, N., Complete Description of Ionization Energy and

Electron Affinity in Organic Solids: Determining Contributions from Electronic Polarization, Energy Band Dispersion, and Molecular Orientation. *Phys. Rev. B* **2015,** *92*, 075145.

33. Yoshida, H., Note: Low Energy Inverse Photoemission Spectroscopy Apparatus *Rev. Sci. Instrum.* **2014,** *85*, 016101.

34. Frisch, M. J.; Trucks, G. W.; Schlegel, H. B.; Scuseria, G. E.; Robb, M. A.; Cheeseman, J. R.; Scalmani, G.; Barone, V.; Mennucci, B.; Petersson, G. A., et al. *Gaussian 09*, Revision A.02; Gaussian, Inc.: Wallingford, CT, USA, 2009.

35. Wang, S. H.; Sakurai, T.; Hao, X.; Fu, W.; Masuda, S.; Akimoto, K., Favorable Electronic Structure for Organic Solar Cells Induced by Strong Interaction at Interface. *J. Appl. Phys.* **2013,** *114*, 183707.

36. Matsuo, Y.; Son, D.; Shimoi, Y.; Marumoto, K., Direct Observation of Spins at Bathocuproine (BCP) Interfaces: An Electron Spin Resonance Study on BCP/Metal (Al or Au) Thin Films. *Chem. Phys. Lett.* **2014,** *607*, 29-33.

37. Bussolotti, F.; Kera, S.; Ueno, N., Potassium Doping of Single Crystalline Pentacene Thin Film. *Phys. Rev. B* **2012,** *86*, 155120.

38. Harada, Y.; Ozaki, H.; Ohno, K., Selective Observation of Outermost Surface-Layer During Epitaxial-Growth by Penning-Ionization Electron-Spectroscopy - Pentacene on Graphite. *Phys. Rev. Lett.* **1984,** *52*, 2269-2272.

39. Hong, Z. R.; Huang, Z. H.; Zeng, X. T., Utilization of Copper Phthalocyanine and Bathocuproine as an Electron Transport Layer in Photovoltaic Cells with Copper Phthalocyanine/Buckminsterfullerene Heterojunctions: Thickness Effects on Photovoltaic Perfonnances. *Thin Solid Films* **2007,** *515*, 3019-3023.

40. Durr, A. C.; Schreiber, F.; Kelsch, M.; Carstanjen, H. D.; Dosch, H., Morphology and Thermal Stability of Metal Contacts on Crystalline Organic Thin Films. *Adv. Mater.* **2002,** *14*, 961-963.

41. Suemori, K.; Yokoyama, M.; Hiramoto, M., Electrical Shorting of Organic Photovoltaic Films Resulting from Metal Migration. *J. Appl. Phys.* **2006,** *99*, 036109.

42. Yoshida, H.; Sato, N., Aluminum Diffusion and Reaction in Thin Films of Perylene-3,4,9,10-Tetracarboxylic Dianhydride: Depth Profiles and Time-Dependent Diffusion Coefficients. *Appl. Phys. Lett.* **2007,** *91*, 141915.

43. Hao, X.; Wang, S. H.; Fu, W.; Sakurai, T.; Masuda, S.; Akimoto, K., Novel Cathode Buffer Layer of Ag-Doped Bathocuproine for Small Molecule Organic Solar Cell with Inverted Structure. *Org. Electron.* **2014,** *15*, 1773-1779.

For Table of Contents Only Graphics